Immunity
Article

Embryonic and Adult-Derived Resident Cardiac Macrophages Are Maintained through Distinct Mechanisms at Steady State and during Inflammation

Slava Epelman,[1] Kory J. Lavine,[1] Anna E. Beaudin,[2] Dorothy K. Sojka,[3] Javier A. Carrero,[4] Boris Calderon,[4] Thaddeus Brija,[1] Emmanuel L. Gautier,[4] Stoyan Ivanov,[4] Ansuman T. Satpathy,[4] Joel D. Schilling,[4,5] Reto Schwendener,[7] Ismail Sergin,[1] Babak Razani,[1] E. Camilla Forsberg,[2] Wayne M. Yokoyama,[3,6] Emil R. Unanue,[4] Marco Colonna,[4] Gwendalyn J. Randolph,[1,4] and Douglas L. Mann[1,*]

[1]Center for Cardiovascular Research, Division of Cardiology, Department of Medicine, Washington University School of Medicine, St. Louis, MO 63110, USA
[2]Department of Biomolecular Engineering, Baskin School of Engineering, University of California, Santa Cruz, Santa Cruz, CA 95064, USA
[3]Division of Rheumatology
[4]Department of Pathology and Immunology
[5]Diabetic Cardiovascular Disease Center
[6]Howard Hughes Medical Institute
Washington University School of Medicine, St. Louis, MO 63110, USA
[7]Institute of Molecular Cancer Research, University Zurich, CH-8057 Zurich, Switzerland
*Correspondence: dmann@dom.wustl.edu
http://dx.doi.org/10.1016/j.immuni.2013.11.019

SUMMARY

Cardiac macrophages are crucial for tissue repair after cardiac injury but are not well characterized. Here we identify four populations of cardiac macrophages. At steady state, resident macrophages were primarily maintained through local proliferation. However, after macrophage depletion or during cardiac inflammation, Ly6c^{hi} monocytes contributed to all four macrophage populations, whereas resident macrophages also expanded numerically through proliferation. Genetic fate mapping revealed that yolk-sac and fetal monocyte progenitors gave rise to the majority of cardiac macrophages, and the heart was among a minority of organs in which substantial numbers of yolk-sac macrophages persisted in adulthood. CCR2 expression and dependence distinguished cardiac macrophages of adult monocyte versus embryonic origin. Transcriptional and functional data revealed that monocyte-derived macrophages coordinate cardiac inflammation, while playing redundant but lesser roles in antigen sampling and efferocytosis. These data highlight the presence of multiple cardiac macrophage subsets, with different functions, origins, and strategies to regulate compartment size.

INTRODUCTION

Cardiovascular disease is the leading cause of adult mortality in the developed world and continues to be a major burden to health care systems. Whether through acute ischemic injury or through the gradual impairment of cardiac function secondary to a variety of clinical pathologies, release of neurohormonal mediators such as angiotensin II (AngII), ultimately leads to irreversible heart failure (Francis, 2011). Data from both animal models and clinical studies show that after cardiac injury, mononuclear phagocytes (MNPs), including monocytes, macrophages, and dendritic cells (DCs), expand within the myocardium. In a context-dependent manner, these cells modulate (either enhance or suppress) the ability of myocardial tissue to recover after injury. Interestingly, both increased or insufficient macrophage expansion impairs infarct healing; however, the exact cell types that might promote injury or enhance tissue regeneration are not known (Nahrendorf et al., 2007; Panizzi et al., 2010).

At steady-state, the traditional view has been that tissue macrophages arise from circulating blood monocytes. Recent studies have demonstrated that tissue macrophages such as microglia, Kupffer cells, and Langerhans cells are established prenatally, arise independently of the hematopoietic transcription factor Myb, and persist into adulthood (Ginhoux et al., 2010; Yona et al., 2013; Schulz et al., 2012). Fate-mapping studies using the pan macrophage marker CX3CR1 confirm the prenatal development of macrophages in many but not all tissues with the notable exception being intestinal CX3CR1^{+} macrophages, which are continually replenished by blood Ly6c^{hi} monocytes (Zigmond et al., 2012). In addition, it is also becoming apparent that tissue-resident macrophages are maintained and can expand dramatically by in situ proliferation, rather than recruitment of blood monocytes (Davies et al., 2013; Jenkins et al., 2011). Such rigorous analysis has not yet been applied to the myocardium. Currently, it is not known what the relationship is between blood monocytes and cardiac macrophages, and which, if any, cardiac macrophage populations are established prenatally. Moreover, how these populations change during cardiac stress and what functions are possessed by individual subsets has not been explored.

Here we characterized cardiac monocytes and macrophages within the myocardium both at steady state and after cardiac

stress. By using complementary in vivo cell tracking, parabiosis, bone marrow transplants and fate-mapping studies, we found the majority of cardiac macrophages were established prior to birth, with significant contribution from yolk sac progenitors. The adult mammalian heart contained specific subsets of both embryonic and adult derived macrophages, which were maintained through local proliferation and replacement by blood monocytes, respectively (see summary, Figure S7). Following the disruption of homeostasis, both within the myocardium and other organs, blood monocyte-derived macrophages were not only recruited, but permanently replaced embryonically established resident macrophage populations. Transcriptional analysis of resident cardiac macrophages revealed that monocyte-derived macrophages coordinate cardiac inflammation, while playing redundant but lesser roles in antigen sampling and efferocytosis.

RESULTS

The Adult Heart Contains Distinct Cardiac Macrophage Subsets

We devised a gating strategy in order to differentiate cardiac macrophages from other immune cells in the myocardium. In addition to cell surface markers, we took advantage of the autofluorescent (Auto) properties of cardiac macrophages in our gating strategy (Figure 1A; and full strategy in Figure S1A available online). The majority of $CD45^+$ cells in the myocardium were $F4/80^+CD11b^+$, and within this heterogeneous population, we found four macrophage subsets. The primary cardiac macrophage populations were $Auto^+Ly6c^-$ and either MHC-II^{hi} or MHC-II^{lo} (R1 or R2, Figure 1A, respectively). Their macrophage identity was confirmed using the highly specific macrophage markers MerTK and CD64 (Figure 1B) (Gautier et al., 2012). MHC-II^{Hi} macrophages were $CX3CR1^{hi}$, $CD206^{int}$, and contained a small subset that was $CD11c^{hi}$, suggesting additional heterogeneity, whereas MHC-II^{lo} macrophages were $CX3CR1^{int}$, $CD206^{hi}$, and $CD11c^{lo}$ (Figure 1B). We identified a third macrophage population that retained Ly6c expression and represented ~2% of total cardiac macrophages (Figure 1A, R3). Monocytes (R4) were found in the $Auto^-$ gate and could be separated from $Ly6c^+$ macrophages (R3) by a lack of MerTK and CD206 expression (Figure 1B). To confirm that these macrophage populations were in the tissue, we injected anti-CD45 intravenously (i.v.) immediately before harvest to label all blood leukocytes (Tagliani et al., 2011). Cardiac macrophages did not label with i.v. anti-CD45, whereas neutrophils, B cells, and a high proportion of $Ly6c^{hi}$ monocytes were labeled, indicating that these cells were in the microvasculature (Figure 1C). Both of the main $Ly6c^-$ macrophage populations (R1 & R2) were larger, more granular, and expressed higher amounts of F4/80 than cardiac monocytes (Figure S1A).

To ensure that our macrophage populations were pure, we needed to adequately account for cardiac DCs. The largest pool of DCs (representing ~1% of total $CD45^+$ cells, R5), were found primarily in the $Auto^-$ gate and were either $CD103^+$ $CD11b^-$ (R6) or $CD103^-CD11b^{hi}$ (R7, Figure 1D). Both DC subsets expressed high amounts of the classic dendritic cell (DC) transcription factor Zbtb46 (Figure 1D) (Satpathy et al., 2012). Because $CD11b^+$ DCs can be difficult to distinguish from macrophages, we determined where these cells appeared in our macrophage gating strategy (Hashimoto et al., 2011). By gating on $CD11b^+Zbtb46^{hi}$ DCs, we found that $CD11b^+$ DCs were $F4/80^-$, and thus fell outside of the macrophage gates (Figure S1B). While MHC-II^{hi} macrophages (R1) contained $CD11c^+$ cells (5%–15%), only a small fraction were $CD103^+$ DCs, and after excluding these $CD103^+$ DCs, the macrophage identity of the remaining R1-$CD11c^{hi}$ subset was confirmed by MerTK expression, consistent with a new fourth cardiac macrophage population (Figure 1E). All cardiac macrophage gates had negligible Zbtb46 signal, confirming that DCs were not significantly contaminating any of our macrophage populations (Figure 1F). We have therefore identified four macrophage subsets in the adult heart (Figure S7B) during steady state, revealing a previously unknown heterogeneity.

Distinct Mechanisms of Cardiac Macrophage Turnover at Steady State and after Disruption of Homeostasis

To determine whether turnover of resident macrophages occurred through replacement by blood monocytes, we created parabiotic mice that differed only by expression of CD45.1 and CD45.2. Blood $Ly6c^{hi}$ monocytes achieved ~30% chimerism over 14 days, which was mirrored by cardiac $Ly6c^{hi}$ monocytes (Figure 2A). After normalizing to blood monocyte chimerism, we found that there was very little replacement of the MHC-II^{hi} or MHC-II^{lo} $CD11c^{lo}$ macrophages, and only modest replacement of $CD11c^{hi}$ MHC-II^{hi} macrophages (R1-$CD11c^{hi}$) by chimeric peripheral monocytes, suggesting that these populations were either locally derived and/or long lived (Figure 2A). $Ly6c^+$ macrophages (R3) had some, but not complete, replacement by monocytes. To confirm these findings, we adoptively transferred $CD150^+$ fetal liver hematopoietic stem cells (HSCs) into animals that were sublethally irradiated in order to reduce, but not extinguish, the resident macrophage populations (Hashimoto et al., 2013). When engraftment was assessed 16 weeks later, we again found that the $CD11c^{lo}$ macrophage populations (R1 and R2) had significantly reduced engraftment rates compared to the other populations, suggesting that these macrophage populations largely persist independent of blood monocyte input (Figure 2B).

To further investigate the mechanisms by which cardiac macrophage populations were replenished, we depleted cardiac monocytes and macrophages with a single i.v. injection of clodronate liposomes. We observed a profound depletion of resident macrophage populations, with a corresponding expansion of $Ly6c^+$ monocytes and neutrophils, which began to decline once macrophages repopulated the myocardium (Figure 2C). To assess the role of blood monocytes in replenishing these macrophage subsets, we labeled blood $Ly6c^{hi}$ monocytes in vivo with fluorescent beads (Tacke et al., 2006) (Figure 2D). Following macrophage depletion, the percentage of $bead^+$ cells increased in all macrophage compartments suggesting that blood $Ly6c^{hi}$ monocytes can differentiate into all macrophage subsets (Figure 2E). In addition, we wondered whether resident macrophages proliferated following depletion. To answer this question, we pulsed animals with bromodeoxyuridine (BrdU) 2 hr prior to harvest to label proliferating cardiac macrophages. In this time frame, proliferating $Ly6c^{hi}$ monocytes remain in the bone marrow and have not been released into circulation (Figure 2F). Following depletion, an increased rate of proliferation was detected in all

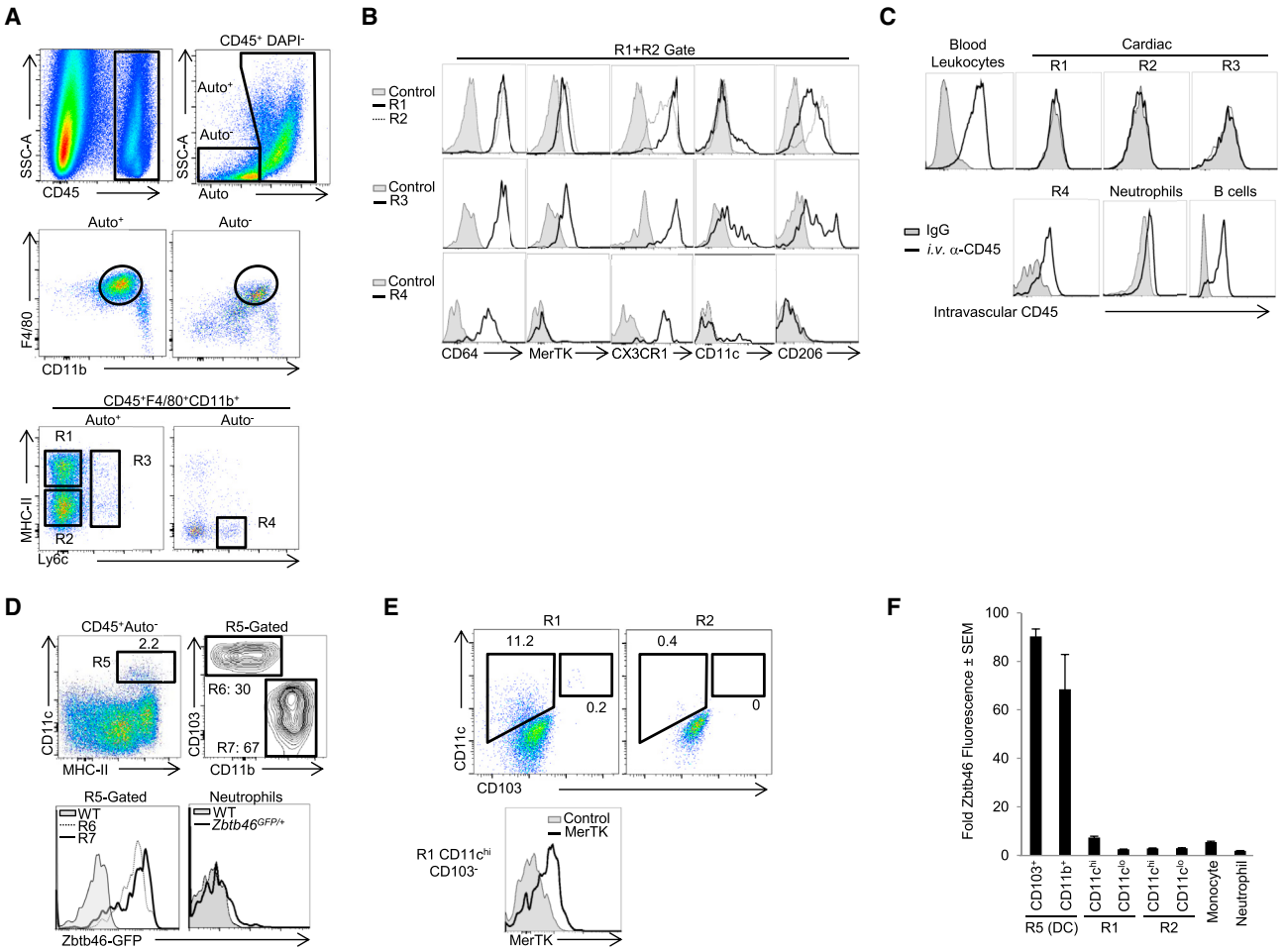

Figure 1. The Adult Heart Contains Distinct Cardiac Macrophage Subsets

Cardiac single cell suspensions were analyzed by flow cytometry. See full gating strategy in Figure S1A.

(A) CD45$^+$ leukocytes were identified, doublets excluded (by FSC-W versus FSC-A) and dead cells excluded by DAPI. Live cells were stratified by autofluorescence (Auto$^+$ or Auto$^-$), gated on F4/80$^+$ CD11b$^+$ myeloid cells and further stratified by MHC-II and Ly6c expression. R1, MHC-II^{hi} macrophages; R2, MHC-II^{lo} macrophages; R3, Ly6c$^+$ macrophages; R4, Ly6c^{hi} monocytes.

(B) Cardiac samples were labeled with isotype control antibody (Control) or with the indicated antibodies. Expression of CX3CR1 was assessed in *Cx3cr1*$^{GFP/+}$ mice and compared with WT mice (Control).

(C) To label intravascular leukocytes, mice were injected i.v. with anti-CD45 and sacrificed 5 min later. Cells were gated as in (A), and intravascular CD45 fluorescence is shown. B cells were B220$^+$ MHC-II$^+$ CD11b$^-$F4/80$^-$ and neutrophils were Ly6g$^+$ CD11b$^+$ F4/80$^-$.

(D) The Auto$^-$ subset contained the majority of cardiac DCs (Total DCs, R5), which were made up of CD103$^+$ CD11b$^-$ (R6) and CD103$^-$CD11b^{hi} (R7) DCs. Zbtbt46-GFP expression was assessed in *Zbtb46*$^{GFP/+}$ mice in R6 and R7, and compared to Ly6g$^+$ neutrophils and WT mice.

(E) Expression of CD11c and CD103 within the primary macrophage gates (R1 and R2).

(F) Relative Zbtbt46-GFP fluorescence ratio in myeloid subsets within the myocardium. The geometric mean fluorescence intensity (gMFI) in each subset in *Zbtb46*$^{GFP/+}$ mice was divided by gMFI of that subset in WT mice. The primary macrophage populations in R1 and R2 were further stratified by CD11c expression. n = 4–8.

See also Figure S1.

macrophage populations except Ly6c$^+$ macrophages (Figure 2G). Together, these data argue that resident CD11c^{lo} MHC-II^{hi} and MHC-II^{lo} macrophages exist separately from blood monocytes during the steady state and are renewed through in situ proliferation. When homeostasis was disrupted following macrophage depletion, Ly6c^{hi} monocytes had the capacity to readily differentiate into these macrophage compartments. In contrast, CD11c^{hi} MHC-II^{hi} macrophages and Ly6c$^+$ macrophages appear to be replenished through both local expansion and monocyte replacement to differing degrees.

Monocyte Recruitment and Local Proliferation Both Drive Cardiac Macrophage Expansion during Stress

The AngII pathway represents a clinically relevant, evolutionarily conserved pathological neurohormonal signaling cascade central to virtually all forms of cardiovascular disease (Francis, 2011). Therefore, we sought to explore the inflammatory effects of AngII on cardiac macrophage populations. AngII induced the rapid influx of Ly6c^{hi} monocytes and subsequent expansion of CD11c^{lo} MHC-II^{lo} (R2) and Ly6c$^+$ macrophages (R3) (Figure 3A; Figure S2A, time course). AngII

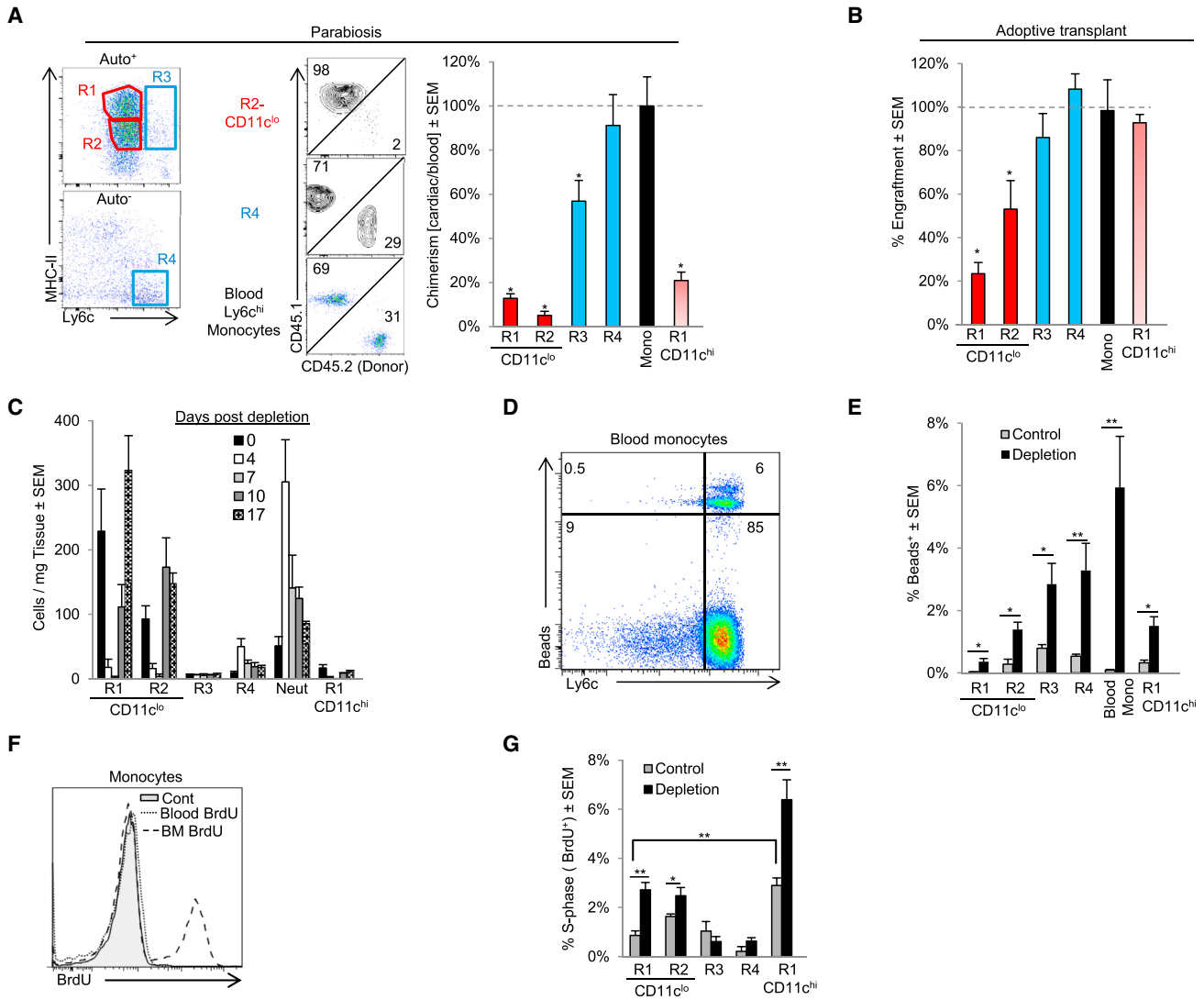

Figure 2. Distinct Mechanisms Regulate Cardiac Macrophage Turnover at Steady State and after Disruption of Homeostasis

(A) CD45.1 and CD45.2 mice were surgically joined to create parabiotic mice and were analyzed after 2 weeks. Dot plots show rate of chimerism for representative populations. The percentage chimerism for each cardiac monocyte and macrophage subset was normalized for the chimeric rate for blood monocytes and expressed as a percentage.

(B) E14.5 Fetal liver CD150^{+} HSCs were sorted and adoptively transplanted into sublethally irradiated mice. Sixteen weeks after transplant, mice were harvested and engraftment of transplanted cells was assessed in blood monocytes and cardiac monocytes and macrophage populations. Engraftment for cardiac populations was normalized for blood monocyte engraftment.

(C–G) Mice were injected with either control liposomes (Control) or liposomes containing clodronate to deplete cardiac macrophages (Depletion) and analyzed over time (C). (D and E) Ly6c^{hi} blood monocytes were labeled with fluorescent microspheres in vivo after macrophage depletion (Tacke et al., 2006). (D) Bead expression in SSC^{lo}CD115^{+}F4/80^{+} blood monocytes after macrophage depletion. (E) Percentage of cardiac bead^{+} cells after depletion. (F) To assess proliferation, mice were injected with BrdU and analyzed 2 hr after injection. Proliferation (BrdU^{+}) in Ly6c^{hi} monocytes in the bone marrow (BM) and blood is shown. (G) Percentage of proliferating BrdU^{+} cells following macrophage depletion (7 days) within the myocardium in each subset. n = 4–7, *p < 0.05. **p < 0.01. Data represents at least two experiments, n = 6–12 mice per group.

induced the expansion of CD11c^{hi} MHC-II^{hi} macrophages (R1-CD11c^{hi}) and a decrease of CD11c^{lo} MHC-II^{hi} macrophages highlighting the dynamic relationship between cardiac macrophage subsets during stress. MerTK and CD64 labeling confirmed the expanded CD11c^{lo} MHC-II^{lo} subset were macrophages (Figure S2B), as were the remaining CD11c^{lo} MHC-II^{hi} macrophages (data not shown). Similar expansion of macrophages was observed after myocardial infarction (Figure S2C). Consistent with AngII as an inflammatory stimulus, Ly6c^{hi} blood monocytes from mice that received AngII upregulated TLR4 and MD-2, and when stimulated with the TLR4 agonist (LPS), produced higher amounts of tumor necrosis factor-α (TNF-α) (Figures S2D and S2E), suggesting peripheral activation occurred prior to infiltration. Thus, the AngII infusion model proved to be a useful system to investigate macrophage dynamics during cardiac stress.

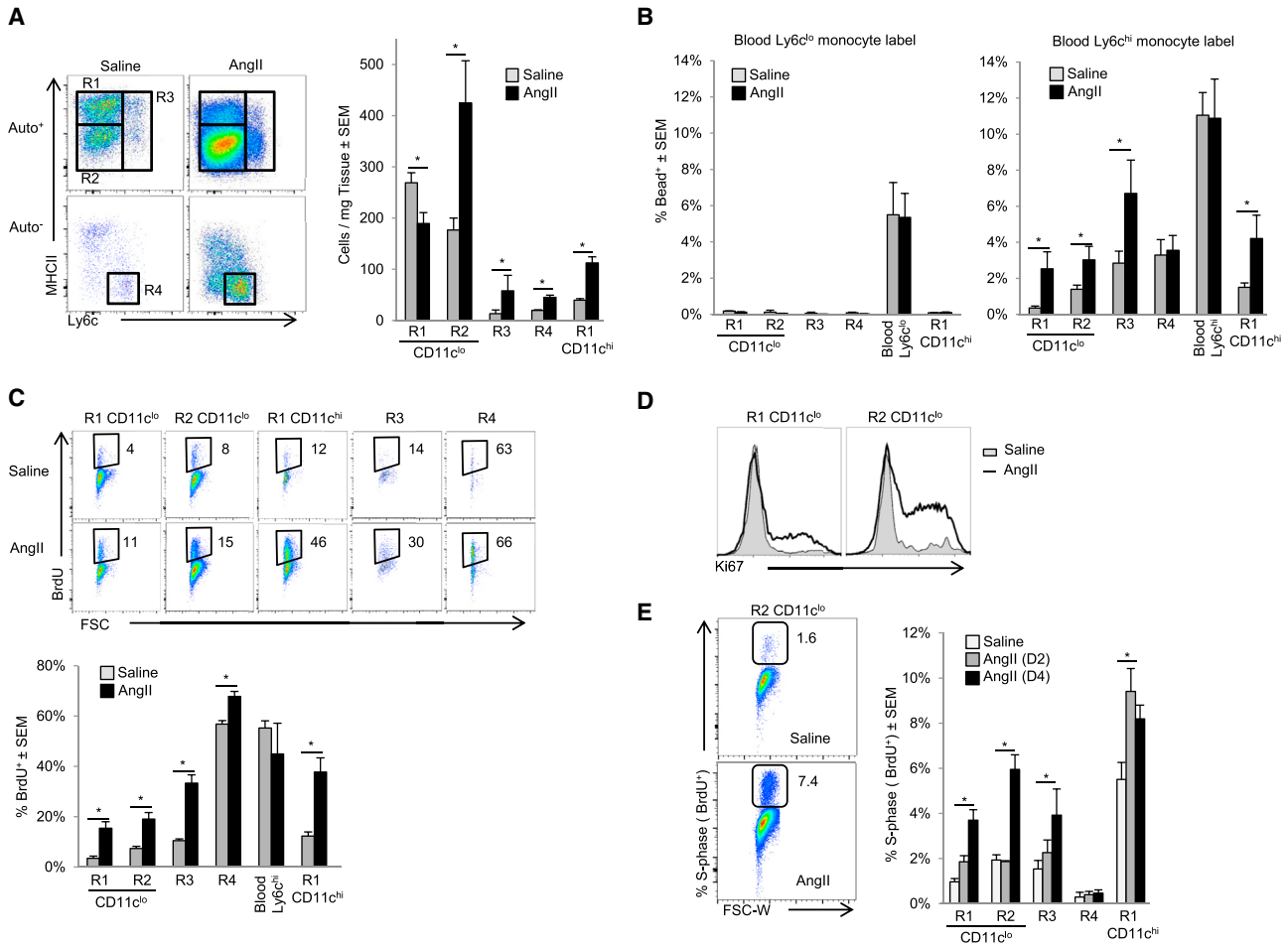

Figure 3. AngII Infusion Induces Numerical Expansion of Cardiac Macrophages through Monocyte Recruitment and Local Proliferation

(A–E) WT mice were implanted with pumps containing either saline or AngII (2 mg/kg/day). (A) Flow cytometric profiles 4 days after infusion gated as in Figure 1A and graphed numerically. (B) Mice with in vivo bead-labeled Ly6c^{lo} or Ly6c^{hi} monocytes were implanted with pumps as above, blood and cardiac tissue was analyzed on day 4, and the percentage of bead^{+} cells is shown. (C) Osmotic pumps containing either saline or AngII (2 mg/kg/day) were implanted and Ly6c^{hi} monocytes were labeled by injecting mice with BrdU 48 and 24 hr prior to harvest. Mice were sacrificed 3 days after pump implantation and BrdU detected by flow cytometry. (D) Intracellular Ki-67 was detected by flow cytometry 4 days after pump implantation as gated in Figure 3A. (E) Percentage of proliferating cells in S phase was assessed by a single BrdU pulse 2 hr prior to harvest. Mice were sacrificed 2 or 4 days after pump implantation. Representative flow cytometric profiles at day 4 in MHC-II^{lo} CD11c^{lo} macrophages (R2) and the percentage of BrdU^{+} cells in each gate. *$p < 0.05$; 2–4 independent experiments, 4–7 mice per group. See also Figure S2.

To determine which subset of blood monocytes (if any) gave rise to cardiac macrophages after AngII infusion, we used the monocyte tracking system described previously, in which fluorescent beads were preferentially phagocytosed by either Ly6c^{hi} or Ly6c^{lo} peripheral blood monocytes (Figure S2F). When Ly6c^{lo} blood monocytes were bead-labeled, there was no enrichment of bead^{+} cardiac macrophages in response to AngII infusion, whereas bead^{+} blood Ly6c^{hi} monocytes gave rise to all macrophage populations (Figure 3B). To confirm these findings, we took advantage of the fact that Ly6c^{hi} monocytes preferentially take up BrdU compared to Ly6c^{lo} monocytes due to their high rate of production and release from the bone marrow (Zhu et al., 2009). After a 2 day BrdU pulse, ~40% of Ly6c^{hi} blood monocytes were labeled. Similarly, there was enrichment of BrdU-labeled cells in all macrophage compartments after AngII infusion (Figure 3C). We confirmed that the progeny of monocytes entered into all macrophage subsets by initially gating on either all cardiac bead^{+} or BrdU^{+} cells and then tracked their contribution to resident macrophage compartments (Figure S2G).

It has become apparent that in addition to monocyte recruitment, macrophages are maintained through local proliferation (Jenkins et al., 2011; Davies et al., 2013). To assess the effect of AngII on local macrophage proliferation, we analyzed expression of Ki-67, a nuclear protein expressed by proliferating cells. At steady state, a relatively high percentage of CD11c^{-} MHC-II^{hi} and MHC-II^{lo} macrophages were Ki-67^{+} (18% ± 2% and 26% ± 2%, respectively), which increased with AngII infusion (Figure 3D). We then quantified macrophages in S phase specifically using a 2 hr BrdU pulse and again found AngII induced proliferation of all macrophage subsets (Figure 3E). Thus cardiac macrophage cell numbers increase during

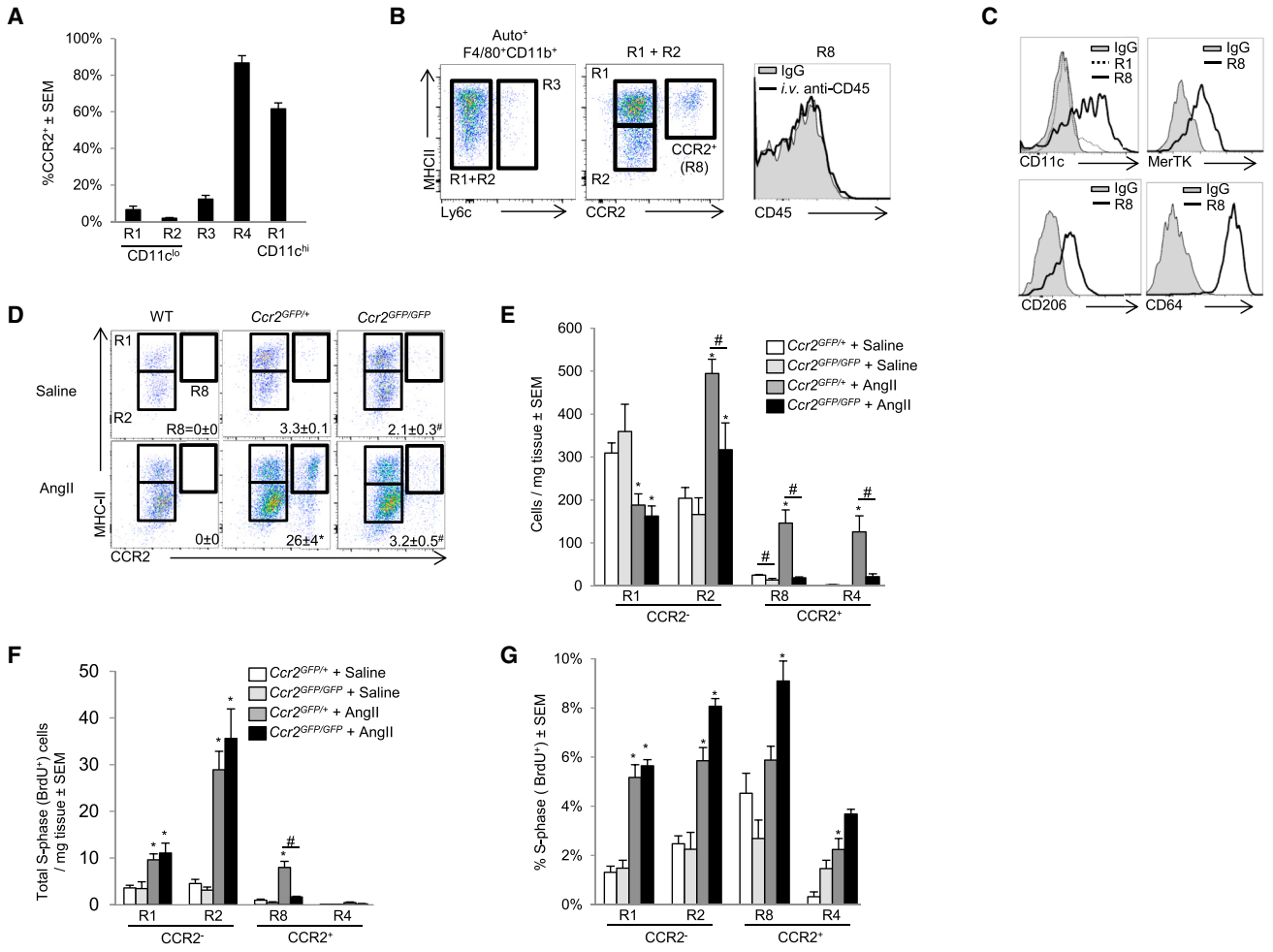

Figure 4. CCR2 Expression Distinguishes Peripheral Monocyte Influx from Proliferating Cardiac Macrophages

(A) Cardiac single-cell suspensions from *Ccr2*$^{GFP/+}$ mice were gated as in Figure 1A and percentage of CCR2$^+$ cells in each gate is shown.

(B) Ly6c$^-$ MHC-II^{hi} and MHC-II^{lo} macrophages were gated together (R1+R2) in order identify CCR2$^+$ macrophages (R8). To determine whether CCR2$^+$ macrophages were extravascular, mice were injected with anti-CD45 i.v. as in Figure 1C and intravascular CD45 expression is shown.

(C) Expression of CD11c, MerTK, CD206, and CD64 was assessed in the regions as outlined.

(D–G) Either saline or AngII (1.5 mg/kg/day) containing pumps were implanted and cardiac tissue analyzed at day 4 in either *Ccr2*$^{GFP/+}$ or *Ccr2*$^{GFP/GFP}$ mice. (D) Cells were gated as in Figure 4B and the percentage of CCR2$^+$ macrophages (R8) is given. (E) Total cell numbers, including gating on cardiac Auto$^-$ Ly6c$^+$CCR2$^+$ monocytes (R4). (F) Total number of proliferating cells (BrdU$^+$, S phase) per mg of tissue after a 2 hr BrdU pulse, and (G) the percentage of cells in S phase in each subset. Two to four independent experiments, four to eight mice per group. *$p < 0.05$ versus saline, #$p < 0.05$ versus *Ccr2*$^{GFP/+}$. See also Figure S3.

inflammation through both recruitment of blood Ly6c$^+$ monocytes and in situ proliferation. Given that monocytes contribute to all macrophage populations during inflammation, it is not possible to separate recruitment from local expansion with cell surface markers alone.

CCR2 Expression Distinguishes Peripheral Monocyte Influx from Proliferating Cardiac Macrophages

To separate expanding resident cardiac macrophages from infiltrating Ly6c^{hi} monocytes, we examined CCR2-deficient (*Ccr2*$^{GFP/GFP}$) mice, which lack peripheral blood Ly6c^{hi} monocytes (Figure S3A) (Serbina and Pamer, 2006). During our initial characterization of *Ccr2*$^{GFP/+}$ mice, we found that cardiac monocytes (R4) were CCR2$^+$ while CD11c^{lo} (R1 and R2) and Ly6c$^+$ (R3) macrophages were CCR2$^-$ (Figure 4A). CD11c^{hi} MHC-II^{hi} macrophages (R1, CD11c^{hi}) were largely CCR2$^+$, allowing us to more easily distinguish the two MHC-II^{hi} macrophage populations (Figures 4A and 4B). Consistent with tissue identity, these CCR2$^+$ macrophages were located within the myocardium and were MerTK$^+$ CD64$^+$ CD11c^{hi} CD206$^+$ (R8, Figures 4B and 4C).

We then compared macrophage numbers during steady state and after AngII infusion in *Ccr2*$^{GFP/+}$ (blood Ly6c^{hi} monocyte sufficient) to *Ccr2*$^{GFP/GFP}$ (blood Ly6c^{hi} monocyte deficient) mice. We examined cardiac CCR2$^+$ and CCR2$^-$ compartments specifically because they allowed us to determine the ability of these populations to regulate macrophage compartment size. In the steady state, cardiac CCR2$^+$ macrophages were reduced (R8) in *Ccr2*$^{GFP/GFP}$ mice, while CCR2$^-$ populations had a normal distribution of CD11c^{lo} MHC-II^{hi} and MHC-II^{lo} macrophages, consistent with their independence from blood monocytes

(Figures 4D and 4E). After AngII infusion, CCR2^{+} MHC-II^{hi} macrophage and CCR2^{+} Ly6c^{hi} monocyte (R4) numbers increased in *Ccr2*$^{GFP/+}$ mice, but not in *Ccr2*$^{GFP/GFP}$ mice (Figures 4D and 4E). CCR2^{-}MHC-II^{hi} macrophages (R1) were rapidly lost during AngII infusion, which was similar between *Ccr2*$^{GFP/+}$ and *Ccr2*$^{GFP/GFP}$ mice and was identical to the loss of CD11c^{lo} MHC-II^{hi} macrophages we previously observed (Figure 3A).

MHC-II^{lo} CCR2^{-} macrophages (R2) had the largest numerical expansion after AngII infusion, and our data suggest expansion occurred through at least two mechanisms. The first was in situ proliferation of resident macrophages. This conclusion was supported by the fact that this compartment expanded in the absence of peripheral monocytes (*Ccr2*$^{GFP/GFP}$ mice, Figures 4D and 4E), and the percentage of macrophages in cell cycle and absolute number of macrophages in cell cycle (S phase, BrdU^{+}) were identical in the absence of peripheral monocytes (*Ccr2*$^{GFP/GFP}$ mice, Figures 4F and 4G). The second mechanism involved the recruitment of CCR2^{+} monocytes that downregulated CCR2 and became CCR2^{-} MHC-II^{lo} Ly6c^{-} macrophages. This conclusion was supported by the fact that blood Ly6c^{hi} monocytes entered that compartment after AngII infusion (Figures 3B and 3C), and when Ly6c^{hi} monocytes were absent (*Ccr2*$^{GFP/GFP}$ mice), the expansion of this compartment was in part blunted (Figures 4D and 4E). Lastly, there was a small expansion of Ly6c^{+} macrophages with AngII, which was composed of mixed populations of CCR2^{+} and CCR2^{-} macrophages and was dependent on blood monocytes (lost in *Ccr2*$^{GFP/GFP}$ mice, data not shown).

Similarly, depletion of cardiac macrophages with clodronate liposomes induced a robust increase in CCR2^{+} MHC-II^{hi} macrophage numbers during the reexpansion phase, which was reduced in *Ccr2*$^{GFP/GFP}$ animals (Figures S3B and S3C). Repopulation of CCR2^{-} macrophages (both MHC-II^{hi} and MHC-II^{lo}) was unchanged in the absence of monocyte recruitment. Together, these data revealed that resident cardiac macrophages (CCR2^{-} CD11c^{lo} Ly6c^{-}) expanded without monocyte input through in situ proliferation, whereas monocytes that expressed CCR2 were able to contribute to both CCR2^{+} and CCR2^{-} macrophage subsets through recruitment and subsequent proliferation.

Adult Cardiac Macrophages Are Established during Embryonic Development

Recent studies have indicated that many tissue-resident adult macrophages are established embryonically and persist separately from the blood monocyte pool (Schulz et al., 2012; Yona et al., 2013; Hoeffel et al., 2012). However, the ontological origin of cardiac macrophages has yet to be explored. Embryonic macrophage populations are established during two phases. Primitive hematopoiesis occurs during early development (E7.5–E11.5), where embryonic yolk sac progenitors develop into either yolk-sac macrophages or red blood cells (Lichanska and Hume, 2000). Later macrophage populations (E11.5–E16.5) arise from fetal liver HSCs through definitive hematopoiesis, which gives rise to all immune lineages, including monocyte-derived macrophages (Kumaravelu et al., 2002; Yona et al., 2013; Hoeffel et al., 2012). Adult brain microglia originate strictly from yolk-sac macrophages (Ginhoux et al., 2010), and although the initial characterization of yolk-sac-derived macrophages suggested a broad persistence of this subset in multiple organs after birth (Schulz et al., 2012), subsequent studies have indicated that fetal liver monocytes might be the primary source at least for skin Langerhans cells and alveolar macrophages, suggesting that the origins of tissue macrophages might be more complex (Hoeffel et al., 2012; Guilliams et al., 2013). To explore the origin of resident cardiac macrophages, we undertook several complementary approaches.

Primitive macrophages seeded the early embryonic heart by ~E9.5 (data not shown) and could be easily detected by ~E10.5 (Figure 5A). These early macrophages were yolk-sac-derived since they appeared in the heart prior to fetal liver hematopoiesis (Hoeffel et al., 2012). Yolk-sac-derived macrophages were MHC-II^{lo}, CX3CR1^{hi}, and had the characteristic F4/80^{hi} CD11b^{lo} expression pattern observed on embryonic yolk-sac macrophages in many tissues (Figure 5B) (Schulz et al., 2012). From ~E12.5 to E16.5, we observed the appearance of a second CX3CR1^{lo} macrophage wave, which had the fetal liver monocyte-derived pattern of F4/80^{lo} CD11b^{hi} in the heart, lung, yolk sac (Figure 5B), and kidney (data not shown). In contrast to the other tissues, where CX3CR1^{hi} and CX3CR1^{lo} macrophages partitioned well by using differential expression of F4/80 and CD11b, cardiac macrophages were universally F4/80^{lo} CD11b^{hi} (Figure 5B), thus indicating a more formal genetic fate-mapping approach would be required to define their ontological origin during development and facilitate analyses of these populations in adulthood.

Self-renewing adult definitive HSCs transiently upregulate FLT3 as they differentiate into all hematopoietic lineages (Boyer et al., 2011). By crossing *Flt3*-cre mice to *Rosa*-mtmg reporter mice, we were able to track cells that either did (TdTom^{-} GFP^{+}; referred to as FLT3-Cre^{+}) or did not (TdTom^{+} GFP^{-}, referred to as FLT3-Cre^{-}) pass through a FLT3^{+} stage and could differentiate definitive HSC-derived macrophages from those that developed independently of HSCs (such as from embryonic yolk sac progenitor or via other, fetal FLT3-independent pathways). To determine which embryonic macrophages were derived from HSCs, we analyzed *Flt3*-cre × *Rosa* mtmg reporter mice at E14.5, a time point at which definitive hematopoiesis has been established in the fetal liver. We found that all F4/80^{hi}CD11b^{lo} (phenotypically yolk-sac-derived) macrophages were entirely FLT3-Cre^{-}, whereas macrophages thought to be derived from fetal liver monocytes (F4/80^{lo}CD11b^{hi}) contained a relatively small population of FLT3-Cre^{+} (~5%) macrophages in all organs tested, suggesting that infiltration of HSC-derived monocytes had begun (Figure 5C). Recombination rates driven by FLT3 were surprisingly low during embryonic development, but by 4 weeks of age, recombination had reached ~85%–95% in blood monocytes (data not shown). We then followed FLT3-Cre^{-} cardiac macrophages over time and demonstrated that they persisted in large numbers in adult mice (20 weeks old) (Figure 5D). We found that only CD11c^{+}CCR2^{+} macrophages were primarily derived from HSC precursors (FLT3-Cre^{+}), whereas the main MHC-II^{hi} and MHC-II^{lo} macrophage subsets (CD11c^{lo}CCR2^{-} Ly6c^{-}) and Ly6c^{+} macrophages originated primarily from FLT3-Cre^{-} pathways (Figure 5D). Comparison of cardiac macrophages to other tissue macrophages demonstrated that with

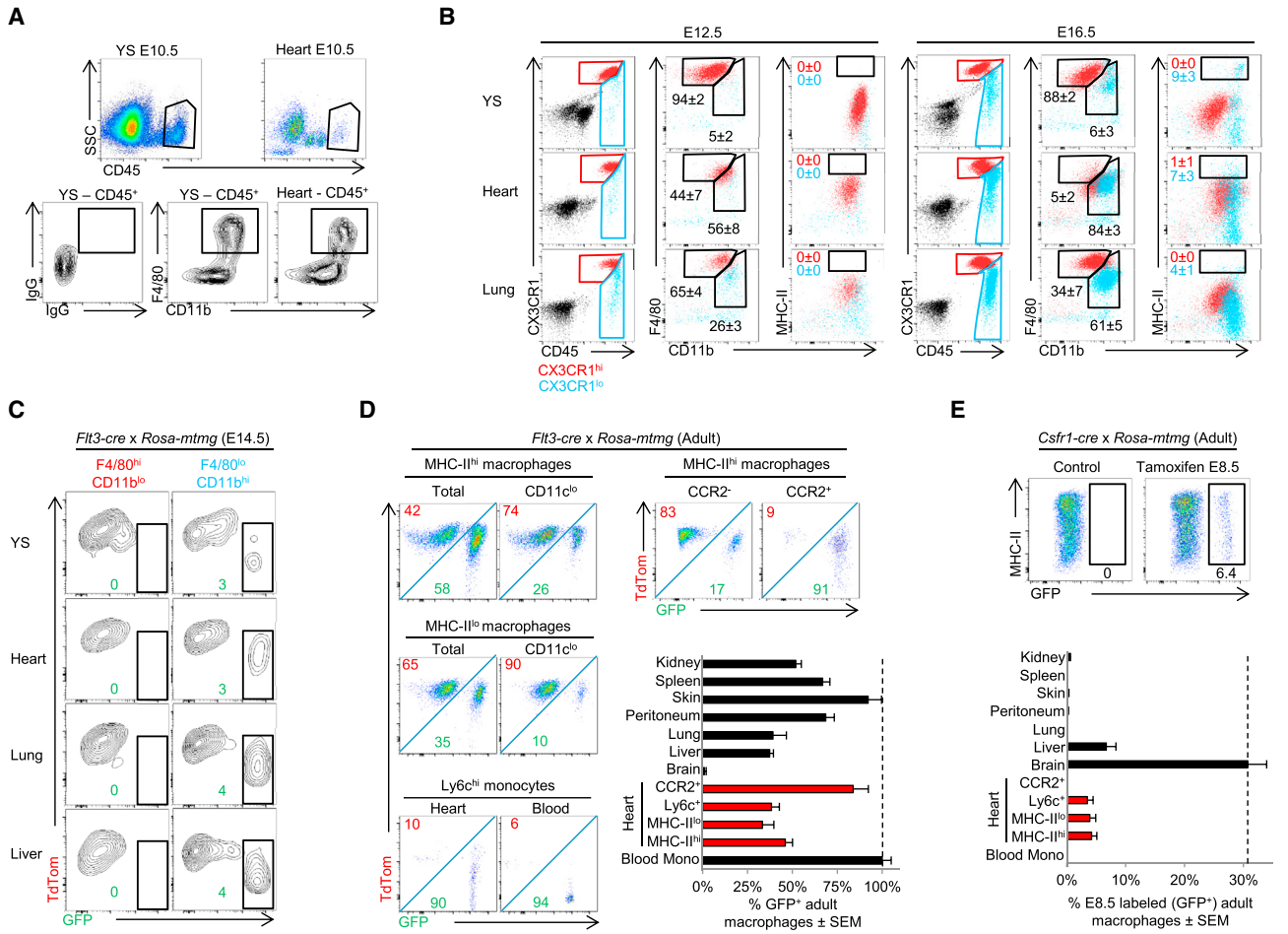

Figure 5. Prenatal Macrophages Colonize the Embryonic Heart and Persist into Adulthood

(A and B) *Cx3cr1*$^{GFP/+}$ embryos were extracted from pregnant females at E10.5, E12.5, or E16.5. (A) Comparison of macrophage populations between the yolk sac (YS) and heart tissue at E10.5. Red color indicates CD45$^+$CX3CR1^{hi} and blue indicates CD45$^+$CX3CR1^{lo} cells. (B) Comparison of yolk sac, heart, and lung macrophages at E12.5 and E16.5.

(C) *Flt3*-cre × *Rosa*-mtmg mice were analyzed for reporter expression (E14.5) in embryonic macrophages from various tissues to determine whether cells had (TdTom$^-$ GFP$^+$) or had not (TdTom$^+$ GFP$^-$) passed through a FLT3$^+$ stage. Two to four litters for each time point with pooled tissue from two to six embryos per animal were used.

(D) Flow plots of adult cardiac macrophage populations in *Flt3*-cre × *Rosa*-mtmg mice. Graphed data represent FLT3-derived cardiac macrophage subsets (red), and other tissue macrophages. Data was normalized to blood monocyte FLT3 recombination, which was typically ~90%. MHC-II^{hi} and MHC-II^{lo} macrophages were gated on the CD11c^{lo} subsets as in Figure 2A. CCR2$^+$ macrophages (R8) were gated as in Figure 4B.

(E) *Csf1r-Mer-iCre-Mer* × *Rosa*-mtmg mice were gavaged with tamoxifen at E8.5 to label the progeny of yolk sac macrophages (TdTom$^-$ GFP$^+$ cells). Mice were sacrificed at 10 weeks of age to determine whether yolk sac macrophage progeny persisted into adulthood. Cardiac macrophages were gated as in (D). Graphed data represent yolk-sac-derived cardiac macrophage subsets (red) and other tissue macrophages. See Supplemental Information for exact gating strategies for each tissue macrophage population. Experiments were repeated at least twice, n = 4–8 animals were group.

See also Figures S4 and S5.

the exception of brain microglia, which were entirely FLT3-Cre$^-$, most adult tissue-resident macrophage compartments contained both FLT3-Cre$^+$ and FLT3-Cre$^-$ subsets (Figure 5D).

The Heart Is One of the Few Adult Organs that Retained Yolk-Sac Macrophages in Significant Numbers

Given the low recombination rates in the embryo, we could not be sure whether in the adult, FLT3-Cre$^-$ resident macrophages were truly FLT3-independent and originated from yolk-sac macrophages (derived outside HSCs), or whether they originated from HSC-dependent fetal liver monocyte pathways. Even if derived from fetal liver monocytes, FLT3-Cre$^-$ cardiac macrophages were not replaced by FLT3-Cre$^+$ blood monocytes in adult animals. To more definitively address this issue, we administered tamoxifen at E8.5 in *Csf1r-Mer-iCre-Mer* × *Rosa* mtmg mice to label yolk-sac-derived macrophages (TdTom$^-$ GFP$^+$) (Qian et al., 2011; Schulz et al., 2012). Approximately ~30% of macrophages within the E10.5 yolk sac were labeled by this approach, reflecting our labeling efficiency (data not shown). Adult brain microglia remained labeled at this ~30% rate, indicating that yolk-sac macrophages labeled at E8.5 persisted faithfully into adulthood. We found that ~5%

of resident cardiac CD11c^{lo} macrophages (both MHC-II^{hi} and MHC-II^{lo}) and Ly6c^{+} macrophages remained labeled in adult mice, whereas CCR2^{+}CD11c^{+} macrophages were not (Figure 5E). Outside of brain microglia, only the heart and liver retained yolk-sac-derived macrophage populations labeled at E8.5, whereas lung, peritoneal, skin, spleen, and kidney macrophages did not (Figure 5E). After normalizing for recombination efficiency, E8.5-labeled yolk-sac macrophages that resided within the adult heart and liver comprised ~15%–25% of their respective resident macrophage pools, indicating that yolk-sac macrophage persistence in adult tissue is much more restricted than is currently appreciated. Mice were not born with MHC-II^{hi} macrophages, but rather these macrophages only developed fully by ~8 weeks of age in a FLT3-independent fashion (Figure S4A), indicating that embryonic MHC-II^{lo} macrophages gave rise to MHC-II^{hi} macrophages after birth. Together, our data suggest that the majority of adult cardiac macrophages developed outside FLT3-dependent pathways and comprised a mixed ontological group containing both embryonic yolk-sac-derived macrophages and fetal monocyte-derived macrophages.

Definitive HSCs Give Rise to Both FLT3-Cre^{-} Tissue Macrophages and FLT3-Cre^{+} Monocytes

Our data also suggested that the absence of FLT3-mediated recombination defines macrophages that originated during embryonic development; however, FLT3 independence might not be able to distinguish between primitive versus definitive hematopoietic macrophage origins during development. As an example, even in the liver lymphocyte pool at E14.5, only 20% of cells had gone through FLT3 pathways, whereas in the adult, FLT3-driven recombination was typically >95% (Figure S4B). This likely reflects rapid proliferation during embryonic development, resulting in less time spent in a FLT3^{+} intermediate and therefore less efficient recombination (Boyer et al., 2011). To investigate further, definitive fetal liver HSCs from *Flt3*-cre × *Rosa*-mtmg mice (FLT3-Cre^{-}) were sorted, adoptively transplanted into sublethally irradiated WT mice, and gated on engrafted cells. As in the embryo, FLT3-mediated recombination was markedly reduced in monocytes shortly after transplant; however, recombination rates increased, and after ~8 weeks had plateaued (Figure S5A). The engrafted cardiac macrophage subsets that were previously identified to be primarily FLT3-Cre^{-} (Figure 5D, CD11c^{lo} MHC-II^{hi} and MHC-II^{lo}) had reduced recombination rates (Figure S5B). Similarly, lung macrophages also had both reduced engraftment rates following irradiation and adoptive transplant (19% ± 6% versus blood monocytes, $p < 0.01$), and by gating directly on these engrafted lung macrophages, we observed reduced FLT3-driven recombination, consistent with their fetal-liver monocyte origin (Figure S5B) (Guilliams et al., 2013). These data suggested that following irradiation, the heart and lung were initially repopulated by FLT3-Cre^{-} blood monocytes that differentiated into long-lasting resident tissue macrophages, because blood monocytes produced at this time had low levels of recombination. Once repopulation was complete, FLT3-Cre^{-} tissue macrophages were not replaced by FLT3-Cre+ blood monocytes over time, even though they both originated from the same engrafted HSC pool.

Because fetal monocytes are an important contributor to long-lived adult cardiac tissue macrophages, we hypothesized that the adult monocyte influx observed after resident macrophage depletion (Figure 2E) could lead to long-term replacement of embryonic (FLT3-independent) macrophages with adult (FLT3-dependent) monocyte-derived macrophages. To address this, we examined *Flt3*-cre reporter mice 6 weeks after macrophage depletion and observed replacement of FLT3-Cre^{-} cardiac macrophages with those derived from FLT3-dependent pathways (Figures S5C and S5D). This durable replacement of embryonically derived macrophages with FLT3-dependent adult monocyte-derived macrophages was even more striking in liver and splenic macrophages, whereas there was no replacement in brain microglia (Figure S5E).

Formal Lineage Tracing Reveals Subset-Specific Recruitment and Expansion Dynamics during Inflammation

We next sought to investigate the dynamics of cardiac macrophage populations in the setting of inflammation by using an ontological approach to clearly distinguish infiltrating adult blood monocytes from embryonically established cardiac macrophages. After AngII infusion, there was expansion of the FLT3-Cre^{-} MHC-II^{lo} macrophage subset and contraction of the FLT3-Cre^{-} MHC-II^{hi} macrophage subset (Figures 6A and 6B), similar to results from experiments with *Ccr2*$^{GFP/GFP}$ mice (Figures 4D and 4E). There was also an increase in the number of cardiac FLT3-dependent MHC-II^{hi} and MHC-II^{lo} macrophages, indicating expansion from monocytes, derived from adult definitive HSC pathways (Figures 6A and 6B). Both FLT3-dependent and independent populations proliferated; thus all macrophages irrespective of their ontological origin had the ability to enter the cell cycle (Figures 6C and 6D).

Adult Monocyte-Derived Macrophages Coordinate Cardiac Inflammation

To gain functional insight into the distinct populations of cardiac macrophages, we sorted the two main CD11c^{lo}CCR2^{-} macrophage populations (MHC-II^{hi} and MHC-II^{lo}) and CCR2^{+}CD11c^{hi} MHC-II^{hi} macrophages and compared them to sorted Ly6c^{hi} blood monocytes. Transcriptional profiling revealed ~4,500 differentially expressed genes (>2 fold) with large differences between macrophages and blood monocytes and, as expected, smaller differences between each macrophage subset (Figure 7A). By using principle component analysis, each macrophage subset clustered separately (Figure S6A). To determine whether cardiac macrophages shared similar genes with other known macrophage populations, we compared differentially expressed genes between monocytes and cardiac macrophages in our data set to those differentially expressed genes between monocytes and representative tissue macrophages in the ImmGen Consortium data set (microglia, lung, and peritoneal macrophages) (Gautier et al., 2012). We found numerous overlapping and nonoverlapping genes across data sets between cardiac macrophages and other tissue macrophage subsets, indicating that cardiac macrophages, like other tissue macrophage populations, possess both common and unique gene-expression patterns (Table S2).

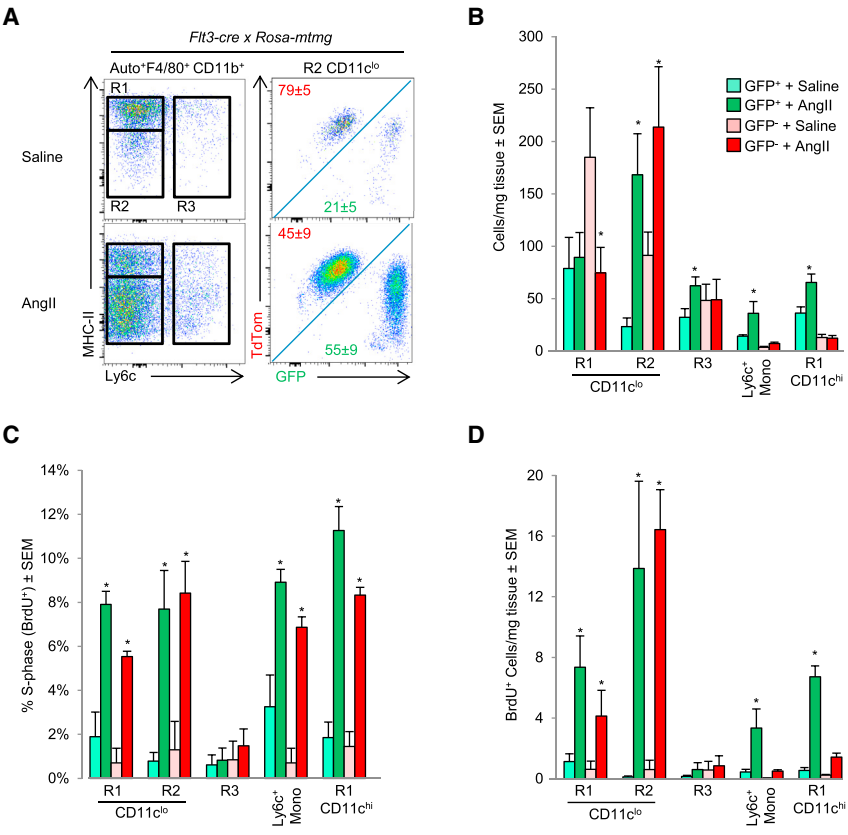

Figure 6. Genetic Lineage Tracing during AngII Induced Inflammation

(A–D) *Flt3*-cre × *Rosa* mtmg mice were analyzed for reporter expression in the myocardium and blood in mice implanted with either saline or AngII containing pumps for 4 days (2 mg/kg/day). (A) Representative flow cytometric plots from MHC-II^{lo}CD11c^{lo} macrophages; and (B) cumulative total cells counts per mg of tissue. (C and D) *Flt3*-cre × *Rosa* mtmg mice were pulsed with BrdU 2 hr prior to harvest. (C) Percentage of cells in S phase, and (D) Total number of cells in S phase in each subset is shown. Red bars indicate FLT3-Cre$^-$ cells (TdTom$^+$ GFP$^-$) and green bars indicate FLT3-Cre$^+$ cells (TdTom$^-$ GFP$^+$). Experiments were repeated at least twice, n = 4–6 animals were group. *p < 0.05 versus saline.

Comparing CCR2$^+$ macrophages to either of the CCR2$^-$ macrophage subsets (MHC-II^{hi} or MHC-II^{lo}) by using Gene Ontology revealed enrichment of immune and inflammatory pathways (see Table S3). The primary distinction between CCR2$^-$ MHC-II^{hi} and MHC-II^{lo} macrophage subsets was related to antigen processing and presentation. Therefore, we focused on the ability of cardiac macrophage subsets to sample antigens. A number of genes involved in endocytosis and intracellular trafficking were differentially expressed (Figure S6B), and there were striking differences in vesicular morphology between the subsets. Compared to Ly6c^{hi}CCR2$^+$ blood monocytes, both CD11c^{lo}CCR2$^-$ [MHC-II^{hi} and MHC-II^{lo}] macrophages were much larger and contained large cytoplasmic compartments that were not present in monocytes, which was particularly apparent in the CCR2$^-$MHC-II^{lo} population (Figure 7B). We next took several approaches to evaluate uptake and processing of antigens in these cells. First, we found that cardiac macrophages were efficient at rapidly internalizing i.v. FITC-dextran in comparison to cardiac DCs and splenic macrophages, and MHC-II^{lo} macrophages were the most efficient cardiac macrophage subset (Figure S6C). To determine whether cardiac macrophages internalized molecules or cells from the surrounding microenvironment in vivo, we analyzed *Rosa*-TdTom × *Mlc2V*-cre mice that express the TdTom reporter strictly in cardiomyocytes, and we also observed increased fluorescence in all cardiac macrophage subsets (Figure 7C). This was extended to an in vitro system where efferocytosis of labeled apoptotic and/or necrotic cardiomyocytes was determined. Similar to the results above, cardiac macrophages, and in particular the MHC-II^{lo} macrophage subset, were efficient at taking up dead cell cargo, suggesting that sampling antigen and uptake of local cardiomyocytes (or material from cardiomyocytes) is a common function of cardiac macrophages (Figures 7C and 7D).

MHC-II-expressing cardiac macrophages were enriched for genes involved in antigen presentation, suggesting that these cells play a role in immunosurveillance (Figure 7E). To test this hypothesis, we either pulsed sorted cardiac macrophage subsets with peptide or we gave them intact protein (which requires uptake, processing, and presentation) and measured their ability to activate T cells. Both cardiac macrophage subsets that expressed high amounts of MHC-II (CCR2$^-$ and CCR2$^+$) were efficient at stimulating T cell responses (whether pulsed with peptide or protein), whereas MHC-II^{lo} macrophages had only a limited ability to activate T cells, despite their robust ability to take up antigen and cells (Figure 7E). CCR2$^+$ macrophages were enriched in genes regulating the NLRP3 inflammasome (Figure 7F), which is responsible for the release of interleukin-1β (IL-1β) and inflammatory responses in multiple tissues, including the heart (Mezzaroma et al., 2011). To investigate the role of CCR2$^+$ macrophages in the production of IL-1β in vivo after AngII infusion, we quantified cardiac IL-1β protein concentrations. As seen in Figure 7F, cardiac IL-1β production was absent in AngII treated *Ccr2*$^{GFP/GFP}$ mice that lack CCR2$^+$ macrophages. Together, these data reveal overlapping and nonoverlapping functions of distinct subsets of resident cardiac macrophages.

DISCUSSION

The long-held belief that blood monocytes give rise to all resident tissue macrophages has been revised by several recent studies. Evidence is emerging that most tissue macrophage populations are established embryonically, persist into adulthood, and turn over through in situ proliferation without significant monocyte input in the absence of inflammation (Schulz et al., 2012; Hashimoto et al., 2013; Yona et al., 2013; Hoeffel et al., 2012; Ginhoux

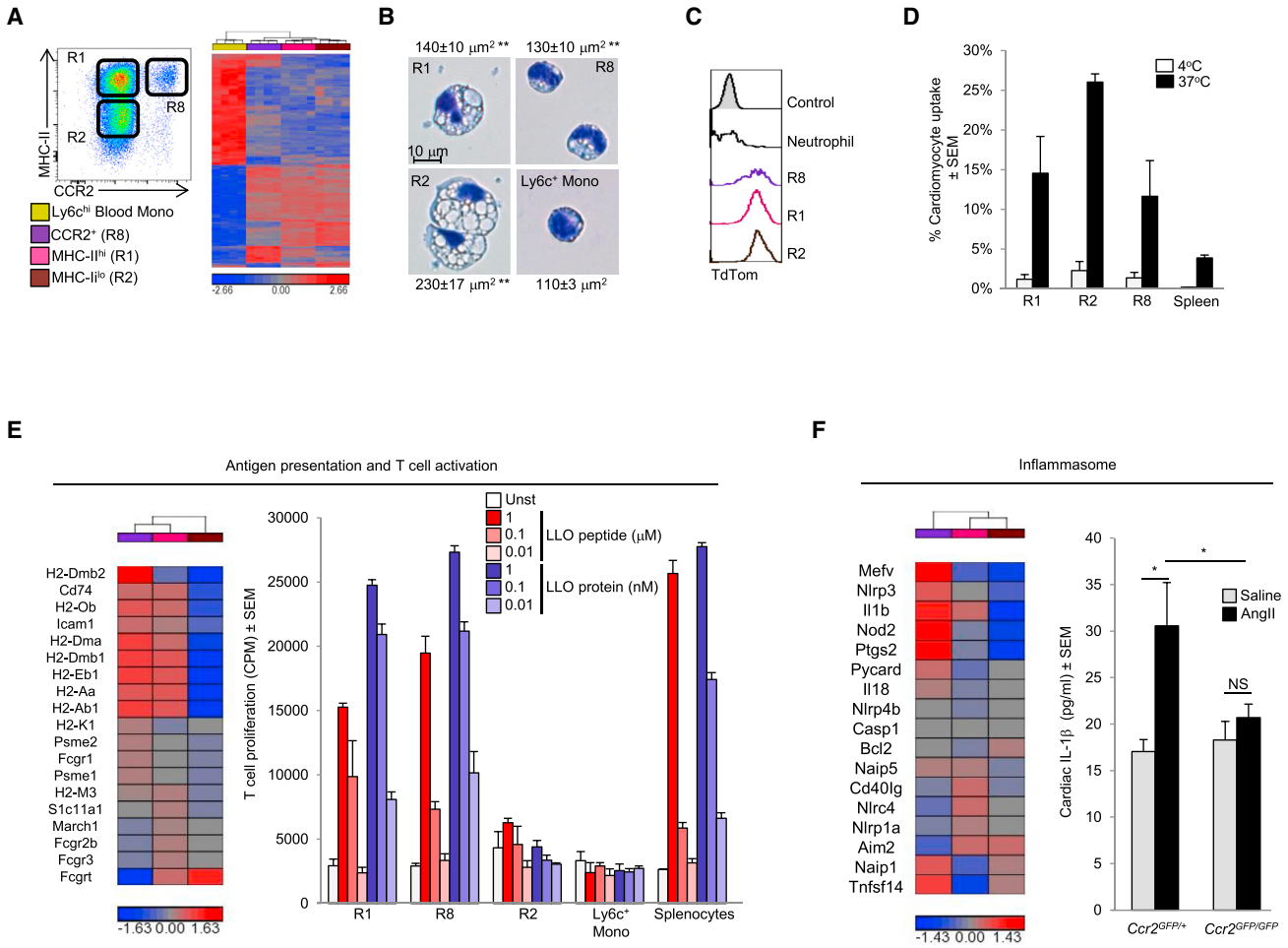

Figure 7. Adult-Derived Macrophages Coordinate Cardiac Inflammation, while Playing Redundant but Lesser Roles in Antigen Sampling and Efferocytosis

Blood Ly6c^{hi} monocytes (yellow), MHC-II^{hi} CCR2^{-} macrophages (R1, Pink) MHC-II^{lo} CCR2^{-} macrophage (R2, brown), and CCR2^{+} MHC-II^{hi} macrophages (R8, purple) were sorted from *Ccr2*$^{GFP/+}$ mice (four replicates), RNA was extracted and global transcriptional profiling performed.

(A) Hierarchal clustering of 4,557 genes differentially expressed in the entire cell population (Fold change > 2).

(B) Sorted macrophage and Ly6c^{hi} blood monocyte subsets were stained with Hema3 solution, surface area was calculated based on an average of at least 20 cells, **$p < 0.01$ versus Ly6c^{hi} monocytes.

(C) Expression of TdTom was determined in cardiac macrophages and neutrophils (Ly6g^{+}CD11b^{+}F4/80^{-}) from cardiomyocyte restricted reporter mice (*Mlc2V*-cre × *Rosa*-TdTom). Control represents background cardiac macrophage fluorescence from WT mice.

(D) Fluorescently labeled apoptotic and/or necrotic cardiomyocytes from WT mice were incubated with cardiac (or splenic) single-cell suspension from *Ccr2*$^{GFP/+}$ mice for 4 hr, at either 4°C or 37°C to assess phagocytic uptake. The percentage of macrophages that took up labeled cardiomyocytes was determined by flow cytometry.

(E) Hierarchical clustering of genes regulating antigen processing and presentation in cardiac macrophages. Sorted cardiac macrophages (as in Figure 7A) were incubated with either Listeriolysin O (LLO) peptide (190–201), or LLO protein (WW nonhemolytic variant), and T cell activation was assessed by IL-2 driven ^{3}H thymidine uptake and expressed in counts per minute (see Experimental Procedures).

(F) Hierarchical clustering of genes regulating inflammasome activation in cardiac macrophages. In vivo cardiac IL-1β production was measured in cardiac tissue lysate from mice (*Ccr2*$^{GFP/+}$or *Ccr2*$^{GFP/GFP}$) infused with either saline or AngII (2 mg/kg/day) for 4 days. Each experiment was repeated at least twice, with three to six mice per group. *$p < 0.05$.

See also Figure S6 and Tables S2 and S3.

et al., 2010). Much less is understood about the precise origin of embryonically established macrophage populations, and their relationship with blood monocytes when homeostasis is disrupted. Here we show that the majority of tissue resident macrophages in adult animals are established embryonically. However, by using fate-mapping studies driven by *Csf1r*, we refine previous analyses and demonstrate that the heart, liver, and brain are the only tissues in which yolk sac-derived macrophages persist into adulthood in substantial numbers. Embryonically established tissue macrophage populations from the lung, spleen, and kidney almost exclusively contain fetal monocyte-derived macrophages. These tissue macrophages are FLT3-Cre^{-}, yet they are not derived from embryonic yolk sac macrophages. Rather, our data indicated that tissue macrophages

are established at a time when definitive hematopoiesis in the fetal liver inefficiently drove FLT3-dependent recombination, thereby allowing these macrophages to be clearly delineated in adult mice because they were not replaced over the long term by FLT3-dependent blood monocytes (see Figure S7). Transplant of fetal liver definitive HSCs revealed that the same progenitor could give rise to both FLT3-Cre$^-$ tissue macrophages and FLT3-dependent blood monocytes. In other words, prior to depletion, embryonically established tissue macrophages are autonomous from blood monocytes. After depletion, and in the setting of competitive resident macrophage proliferation, blood monocyte-derived macrophages have the ability to take up durable residence within tissue and become the dominant macrophage population. After repopulation is complete, tissue macrophage autonomy is restored, albeit with a large complement of adult monocyte-derived macrophages as the new resident macrophage population. Our data brings to light the dynamic nature of monocyte and tissue macrophage plasticity within the setting of an ontological framework that is not well appreciated.

After cardiac injury, recruited monocytes and macrophages play a critical role in healing, with either excessive or insufficient expansion in cell numbers clearly linked to pathology (Nahrendorf et al., 2007; Tsujioka et al., 2009; Panizzi et al., 2010). However, our understanding of resident cardiac macrophage populations and their relationship to blood monocytes is lacking. We found that at steady state, the adult mammalian heart contains two separate and discrete cardiac macrophage pools. The first macrophage pool (CCR2$^-$, CD11c^{lo}) includes the majority of MHC-II^{hi}, MHC-II^{lo}, and Ly6c$^+$ macrophages. These macrophages were separate from the blood monocyte pool and represented an embryonically established lineage made up of progeny from yolk sac macrophages and fetal monocytes. The second macrophage pool was much smaller numerically and was derived from blood CCR2$^+$Ly6c^{hi} monocytes. Thus, there is more phenotypic heterogeneity among cardiac macrophages than previously appreciated (Pinto et al., 2012).

Monocyte and macrophage populations in the heart were also monitored when homeostasis was disrupted. After transient depletion with clodronate liposomes, Ly6c^{hi} monocytes entered the myocardium and were able to differentiate into long-lasting populations of cardiac macrophages. However, proliferation of resident cardiac (CCR2$^-$) macrophages also occurred, indicating that local expansion and recruitment both contribute to macrophages repopulation. Our results with cardiac macrophages differ from observations in the lung, in which macrophages are repopulated through expansion of local lung-tissue macrophages rather than blood monocyte-dependent recruitment (Hashimoto et al., 2013). These data might reflect tissue differences between macrophage subsets and/or depletion techniques. However, our findings were not restricted to the heart, because a near complete and durable replacement of embryonic liver and splenic macrophages was observed after depletion. Repopulation after irradiation was more complex, with more similarities between resident cardiac and lung macrophages. Our data reinforced the observation that resident tissue macrophage populations in the heart and lung could compete effectively with adoptively transplanted monocytes, indicating local macrophage expansion in these niches despite genotoxic injury (Hashimoto et al., 2013). Cumulatively, our data strengthen the notion that redundant pathways underlie macrophage repopulation after depletion in multiple tissue beds and indicate that if expansion by resident embryonically established macrophages is insufficient, bone-marrow-derived monocyte populations become a viable, alternate, tissue macrophage substitute.

Macrophages are thought to play a critical role in the cardiac remodeling response after damage. After AngII infusion, resident cardiac macrophages expand without peripheral monocyte input through in situ proliferation, akin to expansion of pleural macrophages after helminth infection (Jenkins et al., 2011). Infiltrating monocyte-derived macrophages are also able to expand through proliferation, suggesting that proliferation might be a key strategy to regulate macrophage density during inflammation (Davies et al., 2013). Prior studies in ischemic myocardium indicated that recruitment, rather than local proliferation, is the primary mechanism regulating monocyte and macrophage numbers (Leuschner et al., 2012). Our data extend these findings and reveal that multiple cardiac macrophage populations can expand solely through in situ proliferation.

All cardiac macrophage subsets were found to sample their environment by internalizing blood borne or local (cardiomyocyte-expressed) antigens. The subsets that expressed high amounts of MHC-II (CCR2$^+$ and CCR2$^-$ macrophages) efficiently processed and presented antigen to T cells, suggesting a role in immunosurveillance. Alternatively, resident cardiac macrophages, in particular the MHC-II^{lo} subset, are capable of phagocytosing dying cardiomyocytes, thereby contributing to local homeostatic processes. After myocardial injury, inflammasome activation leads to poor tissue regeneration, while blockade of the CCR2 axis prevents ischemic injury (Mezzaroma et al., 2011; Frangogiannis et al., 2007). We observed that numerous genes involved in IL-1β production via the NLPR3 inflammasome were differentially expressed in CCR2$^+$ macrophages and confirmed that IL-1β production in the setting of in vivo cardiac stress was dependent on expansion of CCR2$^+$ monocytes and macrophages. Our data might explain why, in models of cardiac injury, blocking monocyte influx (and thereby subsequent CCR2$^+$ macrophage expansion) is protective, whereas broad macrophage depletion strategies that also target resident CCR2$^-$ cardiac macrophages abolish protection (van Amerongen et al., 2007; Kaikita et al., 2004). Together, these data suggest that preserving resident cardiac macrophage expansion via proliferation, while targeting peripheral monocyte recruitment, might lead to improved myocardial recovery after injury.

In summary, here we demonstrated that the adult mammalian heart contains diverse macrophage populations with distinct ontological origins. Our data define the role of local proliferation and blood monocyte recruitment to the maintenance of these populations at steady state and in response to stress. Moreover, we provide a genetic framework for understanding cardiac macrophage biology in health and disease, which might facilitate further mechanistic and/or therapeutic studies to target subset-specific pathways that contribute to end-organ damage, while leaving cytoprotective pathways intact.

EXPERIMENTAL PROCEDURES

Mice, Tissue Isolation, and Flow Cytometry

The mouse strains utilized in this study are described in detail within the Supplemental Experimental Procedures. Prior to organ collection, mice were sacrificed and perfused with cold phosphate-buffered saline and tissues were minced, digested, and processed into single-cell suspensions as previously described (Nahrendorf et al., 2007) with modifications (see Supplemental Experimental Procedures). Detailed gating strategies, antibodies used, and sorting strategies can be found in the Supplemental Experimental Procedures. All mice were bred and maintained at the Washington University School of Medicine, and experimental procedures were done in accordance with the animal-use oversight committees.

Osmotic Mini-Pump Implantation, Myocardial Infarction Surgery, and Parabiosis

Mice were anesthetized with ketamine and xylazine, the back was shaved and mini pumps (Alzet) containing either saline or angiotensin II (AngII) (Bachem, 1.5–2.0 mg/kg/day) were implanted. The incisions were closed with silk sutures. Complete left anterior descending artery occlusion was performed as previously described (Sondergaard et al., 2010). C57BL/6J and B6-Ly5.1 female mice controlled for age and weight were parabiosed as described (Peng et al., 2013).

Transcriptional Array

Cardiac macrophages (three populations) and Ly6c^{hi} blood monocytes were sorted directly into trizol and the RNA was extracted (QIAGEN). One ng of total RNA was amplified and labeled cDNAs were hybridized to Agilent Mouse 4x44K V2 microarrays. See Supplemental Experimental Procedures for additional details.

Cardiomyocyte Phagocytosis and Antigen-Presentation Assays

Macrophage-mediated uptake of dying cardiomyocytes was performed as previously described (Mounier et al., 2013). Cardiac single-cell suspensions or splenocytes from *Ccr2*$^{GFP/+}$ mice were labeled with cell-surface antibodies and incubated with apoptotic and necrotic cardiomyocytes (at either 4°C or 37°C) in order to distinguish surface binding (4°C) from active phagocytosis (37°C). To assess antigen presentation ability, we plated and incubated sorted cardiac macrophages and Ly6c^{hi} monocytes with either Listeriolysin O (LLO) peptide or LLO protein as previously described (Carrero et al., 2012). A T cell hybridoma specific for LLO was then added and IL-2 production assessed. See Supplemental Experimental Procedures for additional details.

ACCESSION NUMBERS

The GEO accession number for the cardiac macrophage array data reported in this paper is GSE53787.

SUPPLEMENTAL INFORMATION

Supplemental Information includes seven figures, three tables, and Supplemental Experimental Procedures and can be found with this article online at http://dx.doi.org/10.1016/j.immuni.2013.11.019.

ACKNOWLEDGMENTS

Funding for these studies was provided by AHA-SDG-12SDG8030003 (S.E.), NIH K08HL112826-01 (S.E.) and T32HL007081-37 (S.E., K.J.L.), T32CA009547 (D.K.S.), and RO1 HL111094-02 (D.L.M.). We thank Liping Yang for experimental help and advice on parabiosis, Joan Avery and Kassandra Weber for their technical assistance, and Susan Gilfillan for generating the *Ccr2*$^{GFP/GFP}$. This work benefitted from data assembled by the ImmGen consortium.

Received: May 17, 2013
Accepted: November 15, 2013
Published: January 16, 2014

REFERENCES

Boyer, S.W., Schroeder, A.V., Smith-Berdan, S., and Forsberg, E.C. (2011). All hematopoietic cells develop from hematopoietic stem cells through Flk2/Flt3-positive progenitor cells. Cell Stem Cell *9*, 64–73.

Carrero, J.A., Vivanco-Cid, H., and Unanue, E.R. (2012). Listeriolysin o is strongly immunogenic independently of its cytotoxic activity. PLoS ONE *7*, e32310.

Davies, L.C., Rosas, M., Jenkins, S.J., Liao, C.T., Scurr, M.J., Brombacher, F., Fraser, D.J., Allen, J.E., Jones, S.A., and Taylor, P.R. (2013). Distinct bone marrow-derived and tissue-resident macrophage lineages proliferate at key stages during inflammation. Nat Commun *4*, 1886.

Francis, G.S. (2011). Neurohormonal control of heart failure. Cleve. Clin. J. Med. *78* (*Suppl 1*), S75–S79.

Frangogiannis, N.G., Dewald, O., Xia, Y., Ren, G., Haudek, S., Leucker, T., Kraemer, D., Taffet, G., Rollins, B.J., and Entman, M.L. (2007). Critical role of monocyte chemoattractant protein-1/CC chemokine ligand 2 in the pathogenesis of ischemic cardiomyopathy. Circulation *115*, 584–592.

Gautier, E.L., Shay, T., Miller, J., Greter, M., Jakubzick, C., Ivanov, S., Helft, J., Chow, A., Elpek, K.G., Gordonov, S., et al.; Immunological Genome Consortium (2012). Gene-expression profiles and transcriptional regulatory pathways that underlie the identity and diversity of mouse tissue macrophages. Nat. Immunol. *13*, 1118–1128.

Ginhoux, F., Greter, M., Leboeuf, M., Nandi, S., See, P., Gokhan, S., Mehler, M.F., Conway, S.J., Ng, L.G., Stanley, E.R., et al. (2010). Fate mapping analysis reveals that adult microglia derive from primitive macrophages. Science *330*, 841–845.

Guilliams, M., De Kleer, I., Henri, S., Post, S., Vanhoutte, L., De Prijck, S., Deswarte, K., Malissen, B., Hammad, H., and Lambrecht, B.N. (2013). Alveolar macrophages develop from fetal monocytes that differentiate into long-lived cells in the first week of life via GM-CSF. J. Exp. Med. *210*, 1977–1992.

Hashimoto, D., Miller, J., and Merad, M. (2011). Dendritic cell and macrophage heterogeneity in vivo. Immunity *35*, 323–335.

Hashimoto, D., Chow, A., Noizat, C., Teo, P., Beasley, M.B., Leboeuf, M., Becker, C.D., See, P., Price, J., Lucas, D., et al. (2013). Tissue-resident macrophages self-maintain locally throughout adult life with minimal contribution from circulating monocytes. Immunity *38*, 792–804.

Hoeffel, G., Wang, Y., Greter, M., See, P., Teo, P., Malleret, B., Leboeuf, M., Low, D., Oller, G., Almeida, F., et al. (2012). Adult Langerhans cells derive predominantly from embryonic fetal liver monocytes with a minor contribution of yolk sac-derived macrophages. J. Exp. Med. *209*, 1167–1181.

Jenkins, S.J., Ruckerl, D., Cook, P.C., Jones, L.H., Finkelman, F.D., van Rooijen, N., MacDonald, A.S., and Allen, J.E. (2011). Local macrophage proliferation, rather than recruitment from the blood, is a signature of TH2 inflammation. Science *332*, 1284–1288.

Kaikita, K., Hayasaki, T., Okuma, T., Kuziel, W.A., Ogawa, H., and Takeya, M. (2004). Targeted deletion of CC chemokine receptor 2 attenuates left ventricular remodeling after experimental myocardial infarction. Am. J. Pathol. *165*, 439–447.

Kumaravelu, P., Hook, L., Morrison, A.M., Ure, J., Zhao, S., Zuyev, S., Ansell, J., and Medvinsky, A. (2002). Quantitative developmental anatomy of definitive haematopoietic stem cells/long-term repopulating units (HSC/RUs): role of the aorta-gonad-mesonephros (AGM) region and the yolk sac in colonisation of the mouse embryonic liver. Development *129*, 4891–4899.

Leuschner, F., Rauch, P.J., Ueno, T., Gorbatov, R., Marinelli, B., Lee, W.W., Dutta, P., Wei, Y., Robbins, C., Iwamoto, Y., et al. (2012). Rapid monocyte kinetics in acute myocardial infarction are sustained by extramedullary monocytopoiesis. J. Exp. Med. *209*, 123–137.

Lichanska, A.M., and Hume, D.A. (2000). Origins and functions of phagocytes in the embryo. Exp. Hematol. *28*, 601–611.

Mezzaroma, E., Toldo, S., Farkas, D., Seropian, I.M., Van Tassell, B.W., Salloum, F.N., Kannan, H.R., Menna, A.C., Voelkel, N.F., and Abbate, A. (2011). The inflammasome promotes adverse cardiac remodeling following

acute myocardial infarction in the mouse. Proc. Natl. Acad. Sci. USA *108*, 19725–19730.

Mounier, R., Théret, M., Arnold, L., Cuvellier, S., Bultot, L., Göransson, O., Sanz, N., Ferry, A., Sakamoto, K., Foretz, M., et al. (2013). AMPKα1 regulates macrophage skewing at the time of resolution of inflammation during skeletal muscle regeneration. Cell Metab. *18*, 251–264.

Nahrendorf, M., Swirski, F.K., Aikawa, E., Stangenberg, L., Wurdinger, T., Figueiredo, J.L., Libby, P., Weissleder, R., and Pittet, M.J. (2007). The healing myocardium sequentially mobilizes two monocyte subsets with divergent and complementary functions. J. Exp. Med. *204*, 3037–3047.

Panizzi, P., Swirski, F.K., Figueiredo, J.L., Waterman, P., Sosnovik, D.E., Aikawa, E., Libby, P., Pittet, M., Weissleder, R., and Nahrendorf, M. (2010). Impaired infarct healing in atherosclerotic mice with Ly-6C(hi) monocytosis. J. Am. Coll. Cardiol. *55*, 1629–1638.

Peng, H., Jiang, X., Chen, Y., Sojka, D.K., Wei, H., Gao, X., Sun, R., Yokoyama, W.M., and Tian, Z. (2013). Liver-resident NK cells confer adaptive immunity in skin-contact inflammation. J. Clin. Invest. *123*, 1444–1456.

Pinto, A.R., Paolicelli, R., Salimova, E., Gospocic, J., Slonimsky, E., Bilbao-Cortes, D., Godwin, J.W., and Rosenthal, N.A. (2012). An abundant tissue macrophage population in the adult murine heart with a distinct alternatively-activated macrophage profile. PLoS ONE *7*, e36814.

Qian, B.Z., Li, J., Zhang, H., Kitamura, T., Zhang, J., Campion, L.R., Kaiser, E.A., Snyder, L.A., and Pollard, J.W. (2011). CCL2 recruits inflammatory monocytes to facilitate breast-tumour metastasis. Nature *475*, 222–225.

Satpathy, A.T., Kc, W., Albring, J.C., Edelson, B.T., Kretzer, N.M., Bhattacharya, D., Murphy, T.L., and Murphy, K.M. (2012). Zbtb46 expression distinguishes classical dendritic cells and their committed progenitors from other immune lineages. J. Exp. Med. *209*, 1135–1152.

Schulz, C., Gomez Perdiguero, E., Chorro, L., Szabo-Rogers, H., Cagnard, N., Kierdorf, K., Prinz, M., Wu, B., Jacobsen, S.E., Pollard, J.W., et al. (2012). A lineage of myeloid cells independent of Myb and hematopoietic stem cells. Science *336*, 86–90.

Serbina, N.V., and Pamer, E.G. (2006). Monocyte emigration from bone marrow during bacterial infection requires signals mediated by chemokine receptor CCR2. Nat. Immunol. *7*, 311–317.

Sondergaard, C.S., Hess, D.A., Maxwell, D.J., Weinheimer, C., Rosová, I., Creer, M.H., Piwnica-Worms, D., Kovacs, A., Pedersen, L., and Nolta, J.A. (2010). Human cord blood progenitors with high aldehyde dehydrogenase activity improve vascular density in a model of acute myocardial infarction. J. Transl. Med. *8*, 24.

Tacke, F., Ginhoux, F., Jakubzick, C., van Rooijen, N., Merad, M., and Randolph, G.J. (2006). Immature monocytes acquire antigens from other cells in the bone marrow and present them to T cells after maturing in the periphery. J. Exp. Med. *203*, 583–597.

Tagliani, E., Shi, C., Nancy, P., Tay, C.S., Pamer, E.G., and Erlebacher, A. (2011). Coordinate regulation of tissue macrophage and dendritic cell population dynamics by CSF-1. J. Exp. Med. *208*, 1901–1916.

Tsujioka, H., Imanishi, T., Ikejima, H., Kuroi, A., Takarada, S., Tanimoto, T., Kitabata, H., Okochi, K., Arita, Y., Ishibashi, K., et al. (2009). Impact of heterogeneity of human peripheral blood monocyte subsets on myocardial salvage in patients with primary acute myocardial infarction. J. Am. Coll. Cardiol. *54*, 130–138.

van Amerongen, M.J., Harmsen, M.C., van Rooijen, N., Petersen, A.H., and van Luyn, M.J. (2007). Macrophage depletion impairs wound healing and increases left ventricular remodeling after myocardial injury in mice. Am. J. Pathol. *170*, 818–829.

Yona, S., Kim, K.W., Wolf, Y., Mildner, A., Varol, D., Breker, M., Strauss-Ayali, D., Viukov, S., Guilliams, M., Misharin, A., et al. (2013). Fate mapping reveals origins and dynamics of monocytes and tissue macrophages under homeostasis. Immunity *38*, 79–91.

Zhu, S.N., Chen, M., Jongstra-Bilen, J., and Cybulsky, M.I. (2009). GM-CSF regulates intimal cell proliferation in nascent atherosclerotic lesions. J. Exp. Med. *206*, 2141–2149.

Zigmond, E., Varol, C., Farache, J., Elmaliah, E., Satpathy, A.T., Friedlander, G., Mack, M., Shpigel, N., Boneca, I.G., Murphy, K.M., et al. (2012). Ly6C hi monocytes in the inflamed colon give rise to proinflammatory effector cells and migratory antigen-presenting cells. Immunity *37*, 1076–1090.